Water Management

Stage–discharge prediction in straight compound channels using 3D numerical models
Conway, O'Sullivan and Lambert

ice | proceedings

Proceedings of the Institution of Civil Engineers

http://dx.doi.org/10.1680/wama.11.00015
Paper 1100015
Received 10/02/2011 Accepted 08/02/2012
Keywords: hydraulics & hydrodynamics/mathematical modelling/river engineering



ice Institution of Civil Engineers publishing

# Stage–discharge prediction in straight compound channels using 3D numerical models

1 **Philip Conway** BEng, PhD
Doctoral Researcher, School of Civil, Structural and Environmental Engineering, University College Dublin, Dublin, Ireland

2 **John James O'Sullivan** BA, BAI, MSc, DPhil
Lecturer in Hydraulics and Water Engineering, School of Civil, Structural and Environmental Engineering, University College Dublin, Dublin, Ireland

3 **Martin Francis Lambert** BEng, PhD
Professor in Hydraulics and Water Engineering, School of Civil, Environmental and Mining Engineering, University of Adelaide, Adelaide, Australia




**An improved approach for applying three-dimensional (3D) computational fluid dynamics (CFD) models to estimate uniform flow stage–discharge relationships and velocity distributions in straight compound channels is presented. Commonly used modelling approaches tend to be over-specified. For a given flow and water level, desired results are obtained through calibration of resistance coefficients that can be artificially high and vary with changing flow conditions. Furthermore, the momentum interaction at the main channel–floodplain interface is sometimes ignored or is accounted for using a constant eddy viscosity. This potentially results in an overestimation of conveyance capacity in compound channels. The proposed approach represents an advance on these methods and uses a 3D CFD model with $k$–$\varepsilon$ turbulence closure in a predictive capacity where a flow together with physically realistic resistance coefficients are specified. Downstream water levels are then iteratively adjusted until uniform flow conditions are established in the channel. The approach is validated against benchmark experimental data obtained from the large-scale UK Flood Channel Facility and is compared with predictions from divided channel methods.**

## Notation

| | |
|---|---|
| $c_\mu$, $\sigma_k$, $\sigma_\varepsilon$, $C_{\varepsilon1}$, $C_{\varepsilon2}$ | constants for the $k$–$\varepsilon$ turbulence model |
| $f$ | Darcy–Weisbach friction factor |
| $H$ | flow depth |
| $h$ | main channel depth (to bankfull) |
| $i$, $j$ | standard tensor notation indicating the $x$, $y$, $z$ coordinate directions |
| $k$ | turbulent kinetic energy |
| $k_s$ | equivalent sand grain roughness height |
| MS | Manning–Strickler number |
| $n$ | Manning's roughness coefficient |
| $P_k$ | production of turbulent energy |
| $p$ | pressure |
| $Q$ | flowrate |
| $R$ | hydraulic radius |
| Re | Reynolds number |
| $u^*$ | shear velocity |
| $V$ | mean velocity |
| $y$ | distance to the wall |
| $\Delta$ | bedform height |
| $\delta_{ij}$ | Kronecker delta |
| $\varepsilon$ | turbulent dissipation |
| $\kappa$ | von Karman constant |
| $\lambda$ | bedform length |
| $\nu$ | kinematic viscosity |
| $\xi$ | weighting coefficient for the weighted divided channel method |
| $\rho$ | fluid density |
| $\psi$ | bedform steepness |

## 1. Introduction

Compound channels are those that are flanked on either one or both sides by floodplains. These channels are characterised by a momentum interaction between the usually faster moving water in the main channel and the slower moving water in the floodplains (Sellin, 1964). Approaches to analysing compound channels typically consist of dividing the channel cross-section into a number of reasonably homogeneous subsections where velocity distributions are assumed to be uniform and discharges are estimated by the Manning equation or similar formulae. Such

approaches are simplistic and their failure to account for the turbulent momentum exchanges between the main channel and floodplains can overestimate the mean velocity of a compound section relative to an interacting identical channel. This can produce errors in predicted discharges of the order of 25% depending on the method used (Martin and Myers, 1991). Channel slope and geometry also influence the momentum exchange mechanism (Holden and James, 1989). The divisions between the main channel and the floodplains in these divided channel approaches are assumed to be shear-free and are not included in the computation of the wetted perimeter. Myers (1978) questioned the use of shear-free vertical divisions and showed, using boundary shear stress measurements, that an apparent shear force must be present at these boundaries to produce a balance between the gravitational and boundary resistance forces. While vertical divisions between the main channel and floodplains are most common, alternatives such as horizontal and diagonal divisions are also used (Samuels, 1989). Corrections to the divided channel method (DCM) have also been proposed to minimise errors associated with discharge predictions using divided channel approaches with vertical and horizontal divisions. Lambert and Myers (1998) in the weighted DCM, incorporated a weighting factor $\xi$ that biased the floodplain or main channel flow velocities to give a more accurate prediction of the subsection flows. The weighting factor varies between zero and unity and in effect represents an infinite range of channel subdivisions between vertical interfaces ($\xi = 1$) and a horizontal interface at the bankfull division ($\xi = 0$).

However, due largely to their ease of use, DCMs in their standard form are still commonly used in engineering practice. The limitations of basic divided channel approaches with vertical divisions between the main channel and floodplain interface are illustrated in Figure 1 where results from the method are compared with experimental measurements from phase A straight channel tests undertaken at the UK Flood Channel Facility (FCF). The ratio of observed main channel discharges to calculated values using a single channel approach for the inbank test series and divided channel approaches for overbank test series is plotted against relative depth. Relative depth is a non-dimensional parameter used in the analysis of compound channel flows to describe the main channel flow depth relative to the floodplain flow depth. It is generally described as $(H - h)/H$ where $H$ is the total flow depth in the main channel and $h$ is the main channel depth to bankfull. For the inbank test series, measured main channel discharges show good agreement with those determined from the single channel analysis, and a ratio close to unity for all flow depths is obtained. For overbank test series, the dynamic interactions between the main channel and floodplain are shown to produce significant reductions in observed main channel discharges compared to those determined from the DCM. The magnitude of the reduction increases with increasing overbank depth and is significantly more pronounced for the roughened floodplain channel. This demonstrates the influence of the velocity gradient between the slow moving floodplain flow and the faster moving water in the main channel in promoting the turbulent momentum exchanges along the main channel and floodplain interfaces.

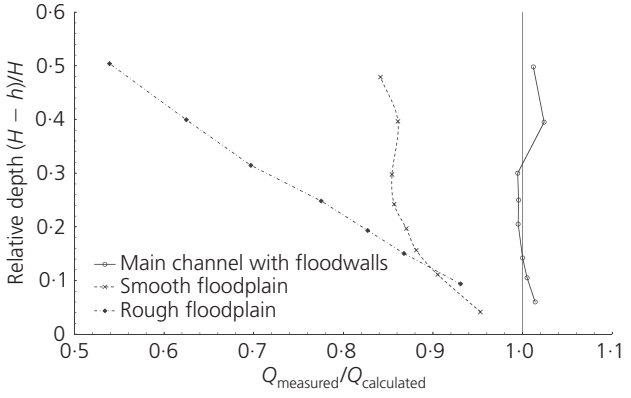


**Figure 1.** Ratio of the observed main channel discharge in the FCF phase A experiments to the calculated discharge using a single channel approach for series 12 (inbank with extended floodwalls) and divided channel approaches for series 2 (smooth overbank) and series 7 (rough overbank)

This 'kinematic' effect, as it is known, takes the form of a bank of large vortices with vertical axes at the main channel edge for relative depths below 0·2. For higher relative depths, secondary flows composed of helicoidal vortices with horizontal axes in the longitudinal direction dominate (Sellin, 1964). Until recently, approaches by engineers to solve many river hydraulic problems typically involved the use of one-dimensional (1D) models (Samuels, 1990). However, these models often fail to account for these complex mechanisms. Advances in computer technologies coupled with the ongoing development of more user-friendly models, have led to an increase in the use of 2D and 3D models. While 2D models have had some success in replicating the kinematic effect (Keller and Wong, 1986), a 3D model is necessary to account for the full complexity of turbulent interactions.

This paper presents a framework within which these higher order computational fluid dynamics (CFD) models can be used to predict stage–discharge relationships and depth-averaged velocity profiles in straight compound channels. Flow and geometry data, together with resistance parameters that define the frictional characteristics of the channel perimeters, form the basis of this prediction. The approach differs from other applications of CFD to compound channel analysis where known stage–discharge curves are used to predict velocity profiles and, in this context, are not being used in a purely predictive capacity to determine stage–discharge relationships.

## 2. Background

In the past, a number of 1D empirical formulae, based on apparent shear stresses acting on particular internal interfaces of

straight compound channels, have been used to predict stage–discharge relationships (Knight and Demetriou, 1983; Knight and Hamed, 1984; Knight *et al.*, 1984; Wormleaton *et al.*, 1982). 2D analytical approaches that implemented depth-averaged parameters have also been developed to yield lateral distributions of both velocity and boundary shear stress (Shiono and Knight, 1991). Keller and Rodi (1988) proposed a 2D numerical approach to establish the distribution of velocity and boundary shear stresses in straight compound channels. In this approach, Nikuradse roughness values for the main channel were adjusted to provide a better average of bed shear stress values. Approaches of this type form the basis of stage–discharge prediction in compound channels using numerical codes in which a parabolic forward marching scheme that requires knowledge of water surface elevations for a range of flow magnitudes is implemented. While 2D methods can provide depth-averaged velocity distributions in compound channels, a study of the degree of dimensionality required to accurately reproduce flow velocities in meandering compound channels by Wilson *et al.* (2003b) showed that the SSIIM (simulation of sediment movements in water intakes with multiblock option) 3D model (Olsen, 2004) produced superior results to 2D codes. Similarly, Rameshwaran and Naden (2004) found that results from Phoenics, a finite-volume 3D model, compared favourably to a 2D model in describing flow fields and predicting bed shear stress values in meandering compound channels.

The aforementioned 3D models applied the $k–\varepsilon$ model (Launder and Spalding, 1974) for turbulence closure. This model has its origins in a desire to improve the mixing length model together with finding an alternative to algebraically prescribing turbulent length scales in moderate- to high-complexity flows. It is a two-equation model that accounts for historical convection and diffusion of turbulent energy (Wilcox, 1993). However, it is limited by its ability to replicate the magnitude of turbulent vortices and secondary currents in cross-field planes. In the modelling of mobile bed compound meandering channel flows using the $k–\varepsilon$ turbulence model, Wormleaton and Ewunetu (2006) replicated pressure-induced secondary circulations in the main channel (Prandtl's first kind) (Demuren and Rodi, 1984). However, the modelling of turbulence-driven secondary motion (Prandtl's second kind) requires non-linear $k–\varepsilon$ models and even they tend to underestimate their magnitude (Sofialidis and Prinos, 1998). Kang and Choi (2006) developed a Reynolds stress model that successfully predicted the mean flow and turbulent features of open channel flow. The model was shown to reproduce the inner and secondary currents at the juncture of the sidewall and free surface in a simple channel. In a comparison between the $k–\varepsilon$ turbulence model, an algebraic stress model (ASM) and an extended ASM that included wall proximity effects, Larsson (1988) found that the ASMs gave marginally superior results to the $k–\varepsilon$ model in replicating measured velocity profiles and the percentage of total shear stress exerted along the main channel and floodplain boundary in a straight compound channel. Jing *et al.* (2009, 2011) successfully simulated turbulent structures in compound meandering channel flows using a Reynolds stress model. However, in a comparison of the $k–\varepsilon$ model and the full Reynolds stress model to measured results, Cokljat and Kralj (1997) concluded that the $k–\varepsilon$ model is capable of predicting the main features of the flow to the acceptable accuracy required in practice. Large eddy simulations (Xiaohui and Li, 2002) have also been implemented in the modelling of compound channels. However, such models are particularly demanding in terms of both computational power and time and their use in river modelling applications is not extensive.

This paper aims to present a framework in which readily available and computationally efficient codes can be used in the prediction of stage–discharge relationships in compound channels to a reasonable degree of accuracy. While the $k–\varepsilon$ model is limited by the assumption of isotropic behaviour, it is generally accepted that second-order turbulence closure models represent an acceptable compromise between accuracy and computational requirements for the hydraulic analysis of most rivers. Furthermore, a number of the codes mentioned above implement a fixed-lid approach. The strength of the model used in this paper lies in the fact that SSIIM was developed as a free-surface code and, as a result, is suitable for the validation of the presented approach.

## 3. Validation of new approach

The usual approach to obtaining stage–discharge relationships for compound channels using numerical codes implements a parabolic forward marching scheme and requires knowledge of water surface elevations for a range of flow magnitudes. In a process known as calibration, the main channel and floodplain hydraulic resistance coefficients are iteratively adjusted for given flow values until the simulated water surface elevation is in agreement with the measured profile (Morvan *et al.*, 2008). Further stage and discharge data are then used to validate the model. The calibration process can result in physically unrealistic roughness coefficients that, in strict terms, are specific only to the calibration flows. Models in this context are not being used in a predictive capacity, but rather are being used to reproduce observed data.

This paper presents an improved approach that uses the hydrodynamic code SSIIM in a predictive capacity to determine stage–discharge relationships in straight compound channels. The proposed approach (Figure 2) better reflects the method followed in experimental tests to establish uniform flow and represents an advance on the usual approaches. The use of physically realistic main channel and floodplain resistance coefficients that are not adjusted eliminates the need for calibration.

The improved approach involves a number of steps. Estimates of appropriate hydraulic resistance values are required to overcome the need for calibration and can be derived from sources such as Cowan (1956) and Hollinrake and Samuels (1995). An arbitrary inflow is selected and a corresponding downstream 'control' depth is assumed. Executing the SSIIM model (or alternative hydro-

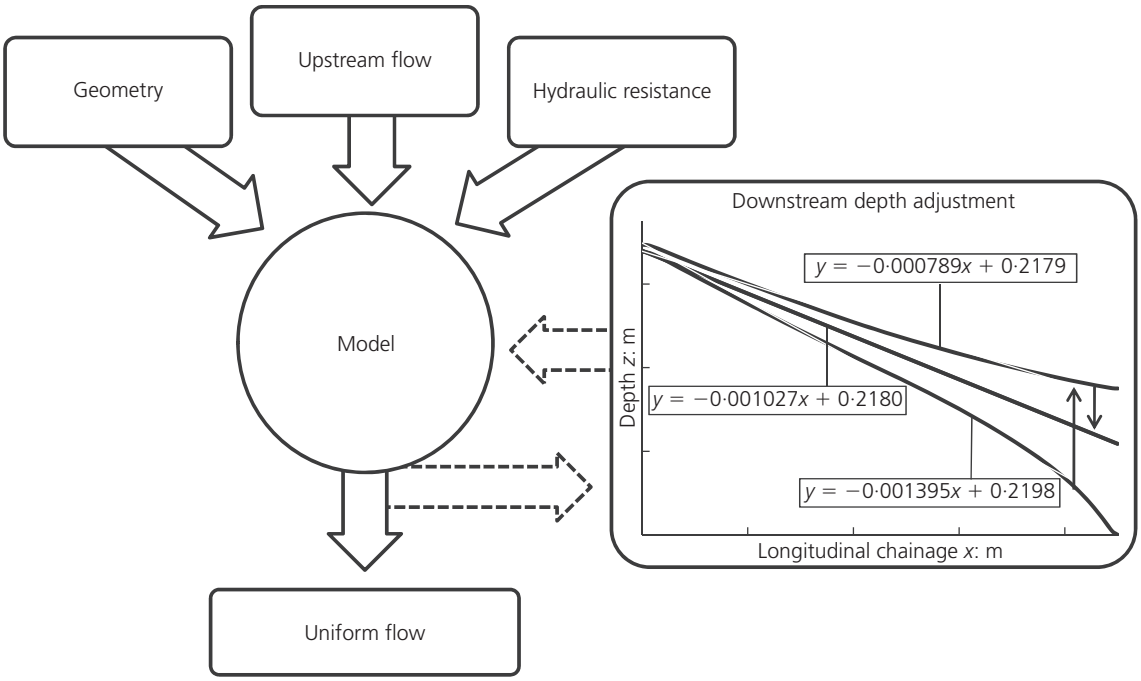


**Figure 2.** Proposed approach showing the three inputs to the numerical code and water surface profile adjustments for different downstream depths to obtain uniform flow conditions

dynamic code) to a converged solution produces a backwater profile. The first iteration from the initially assumed control depth is unlikely to produce uniform flow conditions but a trial and error approach where simulations are repeated for iteratively adjusted downstream depths continues until uniform flow conditions are established. This process is illustrated in the water surface profiles of Figure 2 for the phase A experiments where the required slope is $1{\cdot}027 \times 10^{-3}$. The upper profile has a greater specified downstream depth producing an M1 gradually varied flow profile; the lower profile has a lesser specified downstream depth, producing an M2 profile, and the third profile has the correct downstream depth, resulting in uniform flow conditions. Uniform flow is assumed when the difference between the best-fit line of the water surface and the bed slope is of the order of $10^{-5}$. By repeating this process for a number of assumed flows, a stage–discharge relationship can be constructed.

### 3.1 The UK Flood Channel Facility (FCF)

The revised approach, although applicable to channels of all dimensions and geometries, was benchmarked against the phase A (fixed boundary) and phase C (mobile bed) straight channel dataset from the UK FCF. Details of the phase A experiments have been described by Knight and Shiono (1990) and details of the phase C tests have been reported by Knight *et al.* (1999). The geometrical properties and boundary resistance characteristics for the phase A and phase C experimental channels investigated in this paper are shown in Table 1. The 45 m long phase A channel was formed in screeded concrete and had fixed boundaries. The 40 m long phase C channel was also formed in screeded concrete, but included a mobile bed comprising closely graded, uniform sand with $d_{50}$ and $d_{90}$ values of 0·835 mm and 1·110 mm respectively. Post-construction surveys showed the floodplain or valley longitudinal slopes of the phase A and phase C channels to be $1{\cdot}027 \times 10^{-3}$ and $1{\cdot}834 \times 10^{-3}$ respectively. For the rough floodplain experiments, roughening was achieved from a single configuration of vertical rods, 0·025 m in diameter, arranged in a regular rhomboidal pattern covering the floodplain to a density of 12 rods/m$^2$.

The flow depth for each experiment (discharge) was the average of flow depths determined from digital pointer gauges connected to stilling wells for the length of the channel. These water depths were used to construct the stage–discharge curves for the different channel configurations. Point velocities were measured using a miniature propeller meter. For the phase A tests, main channel velocities were recorded in a grid pattern with vertical and transverse intervals of 0·01 m and 0·1 m respectively. In the phase C tests, point velocity measurements were limited to depth-averaged transverses (40% of flow depth) at intervals of 0·05 m in the main channel and floodplain. Bathymetries for the mobile bed experiments in phase C were recorded using an automatic bed profiler at the conclusion of each test and after which the channel had been drained of standing water. Transverse profiles were recorded at a lateral resolution of 0·025 m for 13 cross-sections at intervals of 1 m between longitudinal chainages of 26 m and 38 m. These data were augmented by three longitudinal

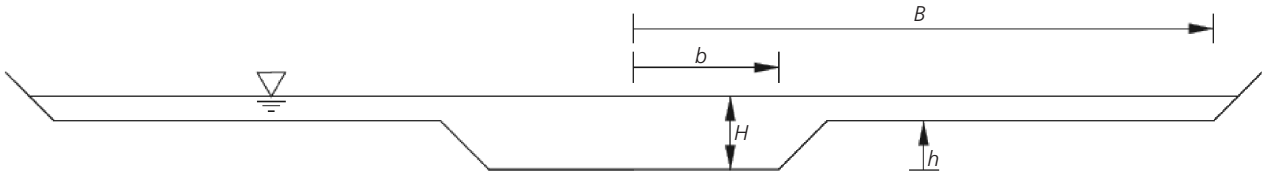


| Series | *B*: m | *b*: m | *H*: m | *h*: m | Main channel | Floodplains |
|---|---|---|---|---|---|---|
| Phase A S2 | 3·15 | 0·75 | 0·1565–0·2880 | 0·15 | Fixed | Smooth |
| Phase A S7 | 3·15 | 0·75 | 0·1559–0·3025 | 0·15 | Fixed | Rough |
| Phase A S12 | 0·75 | 0·75 | 0·1596–0·2988 | 0·15 | Fixed | Isolated |
| Phase C smooth | 4·00 | 0·80 | 0·2249–0·2935 | 0·20 | Mobile | Smooth |
| Phase C rough | 4·00 | 0·80 | 0·2273–0·3202 | 0·20 | Mobile | Rough |

**Table 1.** Channel geometries and properties

profiles measured between these two cross-sections at distances of 0·5, 1 and 1·5 m from the floodplain edge. Although extensive, this grid of data did not fully capture the full detail of the channel bed but did allow accurate estimation of bedform heights and frequencies that were utilised in this study.

### 3.2 Numerical model and boundary conditions

The revised approach was validated using the 3D finite-volume model SSIIM developed at the Norwegian University of Science and Technology (Olsen, 2004). SSIIM solves the 3D Reynolds-averaged Navier–Stokes (RANS) equations for each cell. The equations can be written in Cartesian form as

$$1. \quad \frac{\partial V_i}{\partial x_i} = 0$$

for continuity, and

$$2. \quad \frac{\partial V_i}{\partial t} + V_j \frac{\partial V_i}{\partial x_j} = \frac{1}{\rho}\frac{\partial}{\partial x_j}\left(-p\delta_{ij} - \overline{u_i u_j}\right)$$

for momentum, where $i$ and $j$ represent standard tensor notation indicating the $x$, $y$ and $z$ coordinate directions, $V_i$ is the mean velocity component in the $x_i$ direction, $p$ is the pressure, $\rho$ is the fluid density $\delta_{ij}$ is the Kronecker delta and $-\overline{u_i u_j}$ is the turbulent Reynolds stress, where $u_i$ and $u_j$ are fluctuating velocities, and $\overline{u_i u_j}$ is the Reynolds-averaged value of $u_i u_j$. The first term is the transient term which is neglected by the default algorithm in SSIIM and the second term is the convective term. The third term is the pressure term and the final term is the Reynolds stress term, which requires a turbulence model to be evaluated. The standard $k$–$\varepsilon$ model was used for turbulence closure. The model calculates the eddy viscosity as

$$3. \quad \nu_T = c_\mu \frac{k^2}{\varepsilon}$$

where $c_\mu$ is a constant, turbulent kinetic energy $k = \overline{u_i u_j}/2$ and $\varepsilon$ is the dissipation rate of turbulent kinetic energy. The turbulent kinetic energy $k$ is modelled as

$$4. \quad \frac{\partial k}{\partial t} + V_j \frac{\partial k}{\partial x_j} = \frac{\partial}{\partial x_j}\left(\frac{\nu_T}{\sigma_k}\frac{\partial k}{\partial x_j}\right) + P_k - \varepsilon$$

where $\sigma_k$ is a constant and

$$5. \quad P_k = \nu_T \frac{\partial V_j}{\partial x_i}\left(\frac{\partial V_j}{\partial x_i} + \frac{\partial V_i}{\partial x_j}\right)$$

is a term for the production of turbulence. The dissipation of turbulent kinetic energy $\varepsilon$ is modelled as

$$6. \quad \frac{\partial \varepsilon}{\partial t} + V_j \frac{\partial \varepsilon}{\partial x_j} = \frac{\partial}{\partial x_j}\left(\frac{\nu_T}{\sigma_\varepsilon}\frac{\partial \varepsilon}{\partial x_j}\right) + C_{\varepsilon 1}\frac{\varepsilon}{k}P_k - C_{\varepsilon 2}\frac{\varepsilon^2}{k}$$

where $C_{\varepsilon 1}$, $C_{\varepsilon 2}$ and $\sigma_\varepsilon$ are constants. Recommended values for the five constants in the $k$–$\varepsilon$ model given by Rodi (1980) are hard-coded into the SSIIM software. All simulations were executed under steady-state conditions. SSIIM allows for a control volume method combined with a power-law scheme or the second-order upwind scheme to be used for the discretisation of the convective term. In this research, the second-order upwind scheme (Patankar, 1980) was implemented. Although this scheme is computationally more demanding, it reduces false diffusion

compared to the power-law scheme and has been shown to produce superior results in predicting transverse velocity components in the flow fields of compound channels (Wilson *et al.*, 2003a). The initial free surface is computed using a fixed-lid approach implementing a 1D backwater computation. The backwater profile is computed in a similar way to the single channel method using a Manning–Strickler coefficient, which is related to the roughness height by (Limerinos, 1970)

$$k_s = \left(\frac{26}{\mathrm{MS}}\right)^6 \quad (7)$$

in which $k_s$ is the roughness height in metres, MS is the Manning–Strickler number given by $1/n$ where $n$ is Manning's roughness coefficient. Following commencement of computation, the water surface was updated using the pressure and Bernoulli algorithm. This algorithm is based on the computed pressure field and applies the Bernoulli equation along the water surface to compute the water surface location based on a specified stationary fixed point. In this study, the downstream water level at the channel centreline was used as the fixed point and the water surface profile was updated every 1000 iterations. An investigation into the variation of water surface height between each subsequent update is shown in Figure 3. The change in average water height between the fifth and sixth update (which corresponds to 6000 iterations) was <0·06%. From this analysis, a criterion was set where a minimum of six water surface profile updates was required for the simulated results to be valid. For simulations that converged before 6000 iterations, the number of iterations after which the water surface was updated was reduced until the criterion was satisfied. The Simple method (Patankar, 1980) was used for the pressure and velocity coupling and an implicit solver was used to produce the velocity field across the geometry. Model convergence was assumed when all residuals of the RANS equations and turbulence equations between consecutive iterations were of the order of $10^{-4}$. Convergence at this order is consistent with the literature (Rameshwaran and Naden, 2004).

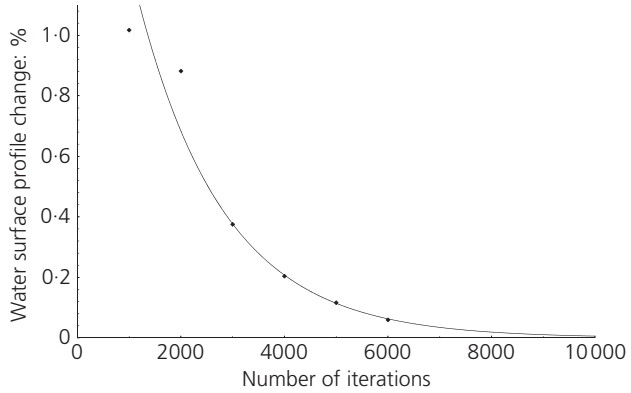


**Figure 3.** Variation in the overall water surface height between two consecutive updates

The numerical simulations were conducted with steady-state boundary conditions consisting of a specified upstream discharge and a specified downstream depth that was adjusted to establish uniform flow conditions. The water velocities and turbulence parameters are prescribed as a Dirichlet boundary condition at the upstream inlet. Zero-gradient boundary conditions are used for all the variables at the downstream outlet. At the water surface, zero-gradient boundary conditions are implemented for all variables except the turbulent kinetic energy, which was set to zero. The side boundary conditions involved a non-slip condition that can result in a steep velocity gradient towards the wall. As an alternative to the excessive grid refinement that is required to model this gradient, the following empirical formula for rough walls (Schlichting, 1979) was used

$$\frac{V}{u^*} = \frac{1}{\kappa}\ln\left(\frac{30y}{k_s}\right) \quad (8)$$

where $V$ is the velocity outside the boundary layer, $u^*$ is the shear velocity, $\kappa$ is a constant equal to 0·4, $y$ is the distance from the wall and $k_s$ is the effective roughness. To ensure the applicability of the wall law, $y^+$ values were kept within the 30–3000 range suggested by literature where $y^+ = u^* y/\nu$ and $\nu$ is the kinematic viscosity. To satisfy this criterion, the mesh resolution was refined at the main channel–floodplain interface and at the outer extent of the floodplains. Mesh configurations for the different test series investigated are summarised in Table 2. The configurations were derived from an investigation (Figure 4) conducted to ensure grid-independent results. Simulated results from a number of different grid densities were compared to measured phase A results, yielding an optimum grid refinement of approximately 100 000 cells, which corresponds to approximately 150 000 cells for the larger phase C channel. The upper curve in Figure 4 shows a comparison of the measured flow distribution between the main channel and the floodplain to that predicted by the numerical code. The lower curve relates the measured water surface profile to that predicted in the simulation. Water surface responsiveness to grid refinement is quite low, which is in agreement with an investigation into optimal mesh size carried out by Ettema (2011).

### 3.3 Modelling of boundary roughness

In this paper, the hydraulic resistance for the screeded concrete finish of the FCF was obtained from the smooth boundary law

$$\frac{1}{f^{1/2}} = C\log[\mathrm{Re}(f^{1/2})] + D \quad (9)$$

where $f$ is the friction factor, Re is the Reynolds number and Ackers (1991) obtained values of 2·02 and −1·38 for $C$ and $D$

| Series | Number of *i* gridlines | Number of *j* gridlines | | | Number of *k* gridlines | Total number of cells |
|---|---|---|---|---|---|---|
| | | Main channel | Floodplain | Side walls | | |
| Phase A | 226 | 20 | 44 | 11 | 7 | 99 900 |
| Phase C | 201 | 18 | 62 | 13 | 9 | 147 200 |

**Table 2.** Details of computational meshes: *i*, longitudinal direction; *j*, lateral direction; *k*, vertical direction

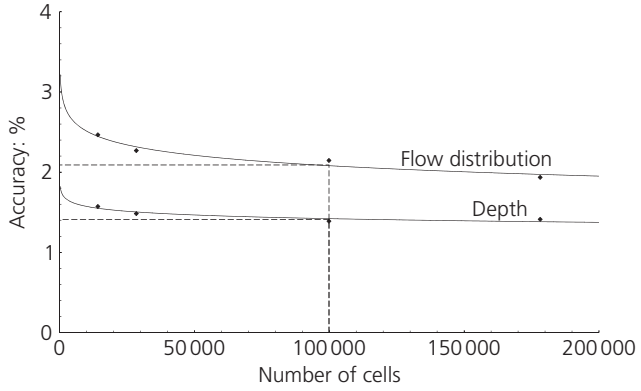


**Figure 4.** Grid refinement investigation

respectively. The value of $f$ in Equation 9 was converted into a $k_s$ value required by SSIIM using an equation formulated for rough turbulent pipe flow and extended for open channel flow applications (Colebrook, 1939)

$$10. \quad \frac{1}{f^{1/2}} = C \log\left(\frac{R}{k_s}\right) + D$$

where $C$ and $D$ have values of 2·0 and 2·34 respectively and $R$ is the hydraulic radius.

The rod roughness method of Ackers (1989) was used to predict the flow resistance for tests undertaken with roughened floodplains. The method is based on a developed set of formulae that allows for different numbers of rods of specified diameter and of known spacing arranged in alternate rows. The mobile main channel bed of the phase C FCF tests introduces an extra degree of freedom into the modelling process. Sediment movement increases the complexity of compound channel flows by facilitating the creation of bedforms, which increase flow resistance. The shape characteristics of these bedforms and their associated roughness are known to depend on channel stage and geometry and vary with flow conditions (Simons and Richardson, 1961). The approach used in this paper to obtain main channel resistance values for the mobile channel is similar to the divided resistance approaches of Engelund (1966) and more recently Shen *et al.* (1990) where the individual influences of skin (or grain) and form resistance are isolated such that their sum approximates to the total channel resistance. Van Rijn (1984) proposed the following relationship for the equivalent sand grain roughness

$$11. \quad k_s = 3d_{90} + 1{\cdot}1\Delta(1 - e^{-25\psi})$$

where $\Delta$ is the average bedform height, $d_{90}$ is the average sediment size, for which 90% of the material (by weight) is finer, $\psi = \Delta/\lambda$ represents the steepness of individual bedforms and $\lambda$ is the average bedform length. Average bedform heights and lengths for each of the phase C tests were estimated from longitudinal bed profiles recorded with an automated bed profiler at the conclusion of each test when all water was drained from the test section of the facility. The sediment grain size and the measured bedform dimensions were then used to compute the mobile bed channel boundary roughness for each test using Equation 11.

### 3.4 Results

The new approach was validated against benchmark straight channel data from the UK FCF. Predicted stage–discharge relationships were constructed by assuming a discharge and obtaining the corresponding depth from the numerical model. This process was repeated for a number of assumed flows and the resulting relationship together with main channel and floodplain transverse velocity profiles and flow proportions were compared to the measured data and results calculated using the DCM for each flow. The validation included phase A and C compound channel flows in fixed and mobile bed channels with both smooth and rod-roughened floodplains. Figure 5 shows the stage–discharge relationships for the four overbank test series in Table 1. The results show that the new approach predicts stage–discharge relationships reasonably well. The depth for a given discharge is overestimated by around 2% for the smooth phase A channel and 5% for the roughened test case. The $k$–$\varepsilon$ model seems to work best for relative depths of around 0·3, which coincides with the range where vortices with vertical axes are replaced by secondary flows composed of helicoidal vortices with horizontal axes at the interface. The DCM results for the smooth test case are quite good, with predicted depths being underestimated for given flows by an average of approximately 3%. Errors increase significantly for the roughened floodplain tests to average values of approximately 9%, with the largest underestimations of around 20% being observed at the highest flow depths. Errors of this

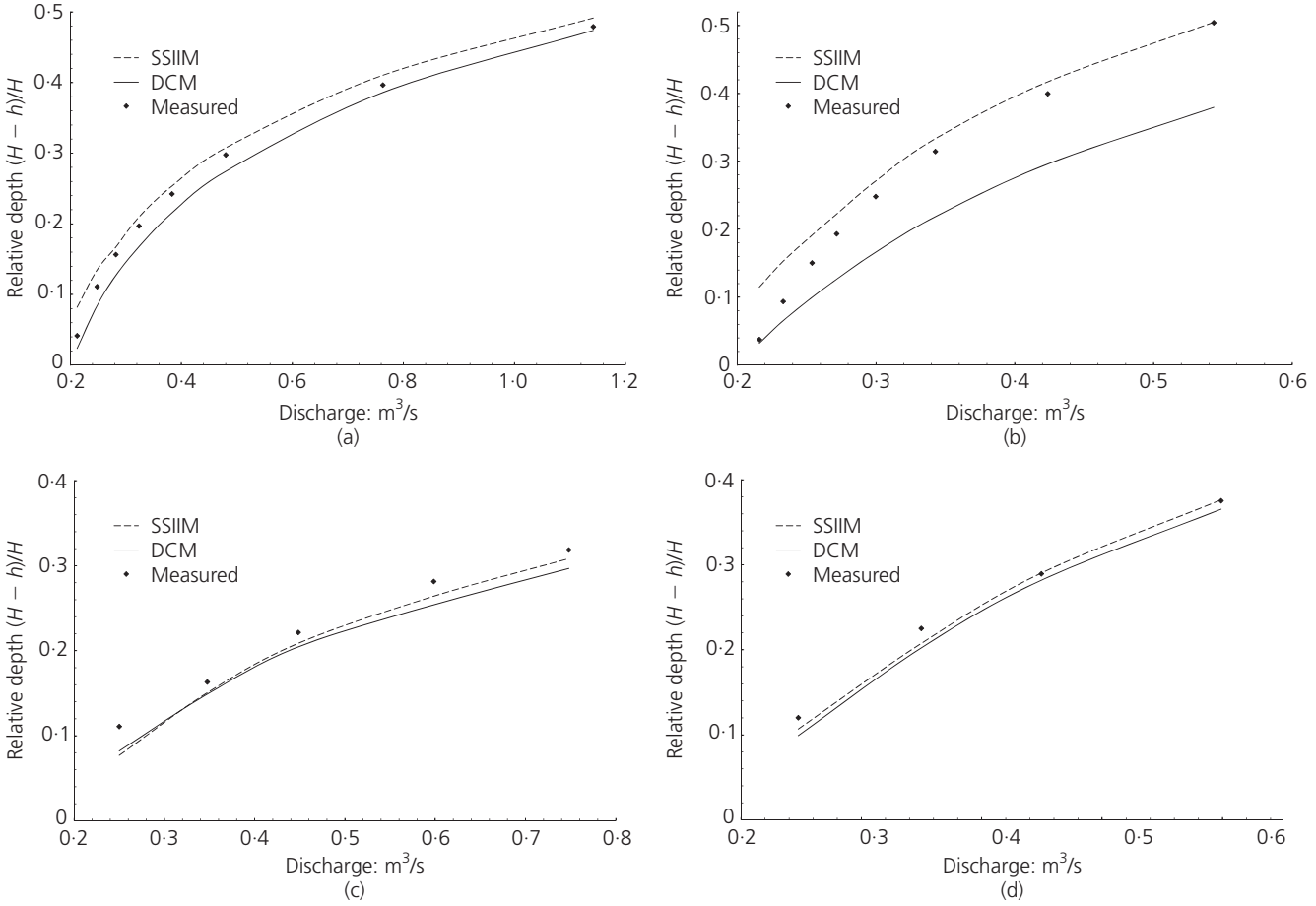


**Figure 5.** Comparison of predicted (SSIIM), calculated (DCM) and measured (FCF) stage–discharge relationships for (a) phase A smooth channel, (b) phase A rough channel, (c) phase C smooth channel and (d) phase C rough channel

magnitude are consistent with those reported in the literature and reflect the failure of the DCM to account for turbulent momentum exchanges along the interface between the main channel and floodplain zones (Lambert and Myers, 1998). DCM errors of approximately 2 and 3% respectively were observed for the roughened and smooth floodplain test cases of the mobile bed phase C channel, compared with less than 1 and 2% respectively for the predicted results using SSIIM.

Velocity contours predicted by SSIIM using the new approach are compared to those from measured values in Figure 6 for two phase A tests of relative depth 0·3 with both smooth and rough floodplains. Good agreement is shown between the measured and predicted values. For the measured contours of the roughened test case, maximum streamwise velocity occurs below the water surface and the velocity contour lines bulge towards the corners. These are characteristic features of secondary flows (Matthes, 1947) and are not replicable by the isotropic $k$–$\varepsilon$ model. However, the momentum transfer from the main channel to the floodplain is evident in both measured and predicted results for the roughened test case. Main channel velocity magnitudes are reduced compared with the magnitudes for the main channel of the smooth floodplain despite the main channel resistance remaining identical; this confirms a momentum transfer from the main channel to the reduced floodplain velocities caused by the roughness elements.

Depth-averaged velocities for the phase A and C smooth and rough channel are shown Figure 7 for relative depths of $\cong$0·3. Results for the phase A experiments (Figures 7(a) and 7(b)) best reflect the limitation of the DCM approach in not accounting for the turbulent momentum exchange at the main channel and floodplain interfaces. Velocity values that exceed measured values and corresponding floodplain velocities that are lower than measured values are observed. However, the influence of the momentum transfer from the faster moving main channel to the lower velocity floodplain flow is better captured by the SSIIM hydrodynamic code. An interesting feature of the smooth floodplain combined with a mobile bed is the development of a negative velocity differential from the main channel to the floodplain.

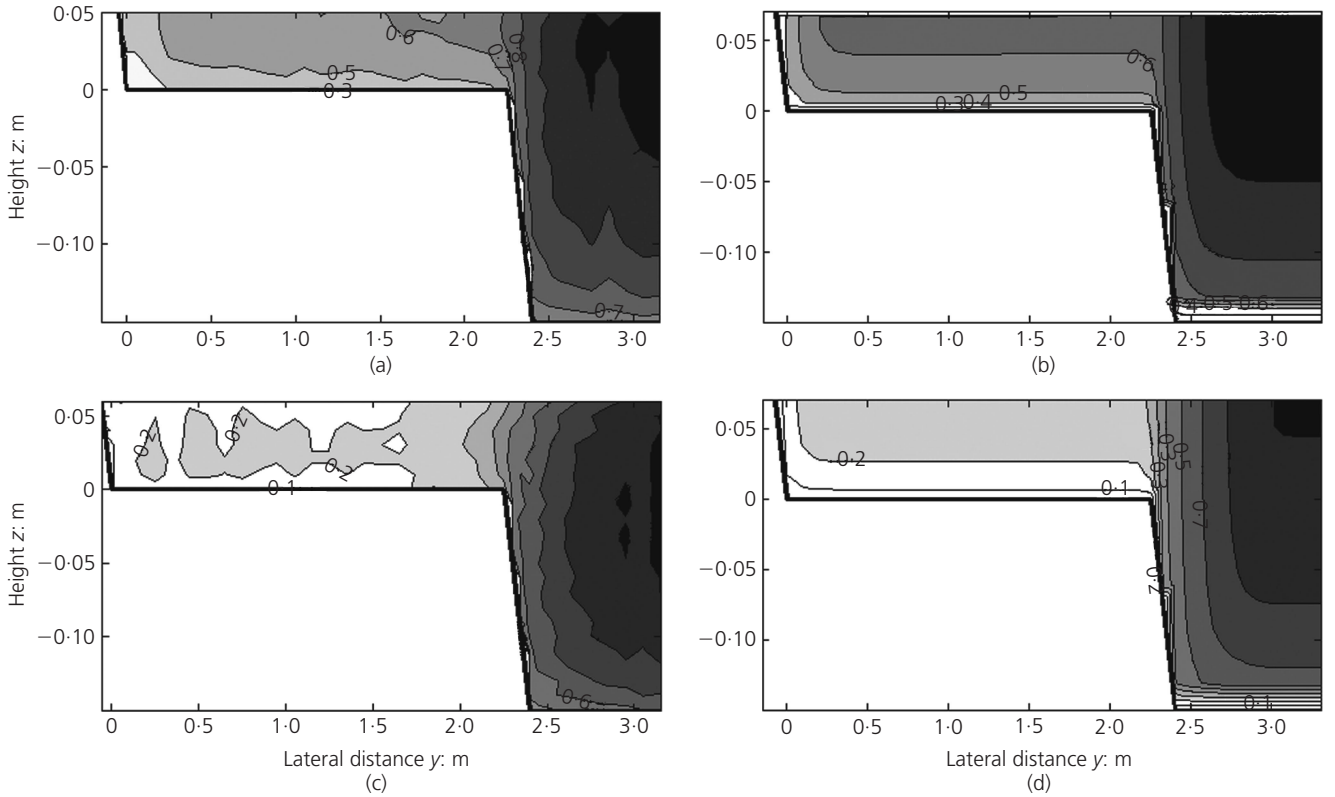


**Figure 6.** Comparison of velocity contours for (a) measured phase A smooth channel, (b) predicted phase A smooth channel, (c) measured phase A rough channel and (d) predicted phase A rough channel

While improbable in nature, both the DCM and SSIIM capture this reversal in peak velocity. The velocity is, however, near-uniform between the floodplain and the main channel, resulting in a much reduced momentum transfer. Consequently, calculated results from the DCM are quite similar to those measured and predicted by SSIIM. A source of error in the measured data manifests itself at the outer extent of the roughened floodplain where the increase in velocity is attributable to leakage outside of the test area.

An integration of respective depth-averaged velocities laterally for each given flow produced the main channel and floodplain flow proportions in Figure 8. Predicted results obtained from the revised modelling approach with SSIIM provide a better fit to the measured data for the phase A experiments than those calculated using the DCM. The method underestimates floodplain flow proportions and overestimates main channel magnitudes due to its inability to replicate the mechanism from which main channel flow would be transferred to the slow moving floodplain zone. Errors in DCM estimates that result from increased velocity gradients across the channel subsections are again shown to be greater for the roughened floodplain tests. As a result of skin and form resistance in the mobile bed main channel, hydraulic resistance values exceed those that describe the smooth floodplains. This situation produces conditions where the mean velocity in the floodplain exceeds that in the main channel and, as reported by Myers (1978), this reverses the direction of the momentum transfer so that it now occurs from the floodplain to the main channel. As a result, the DCM is shown to marginally underestimate the velocity and discharge in the main channel and overpredict the same parameters in the floodplains. Overall, DCM and SSIIM results are quite similar for the mobile test case and reflect the observed results in Figure 7.

Turbulent kinetic energy plots are presented in Figure 9. The turbulence at the interface is easily identifiable, confirming that, while the $k$–$\varepsilon$ turbulence fails to replicate turbulence-driven secondary flows in cross-stream planes, it does account for some of the turbulent interaction. The higher turbulent kinetic energy at the main channel and floodplain interface for the roughened floodplain test cases compared with that for the smooth floodplain tests is significant and reflects the influence of the velocity differential between these channel zones in promoting the turbulent momentum interactions. A significant generation of turbulent kinetic energy is also observed at the mobile bed boundary.

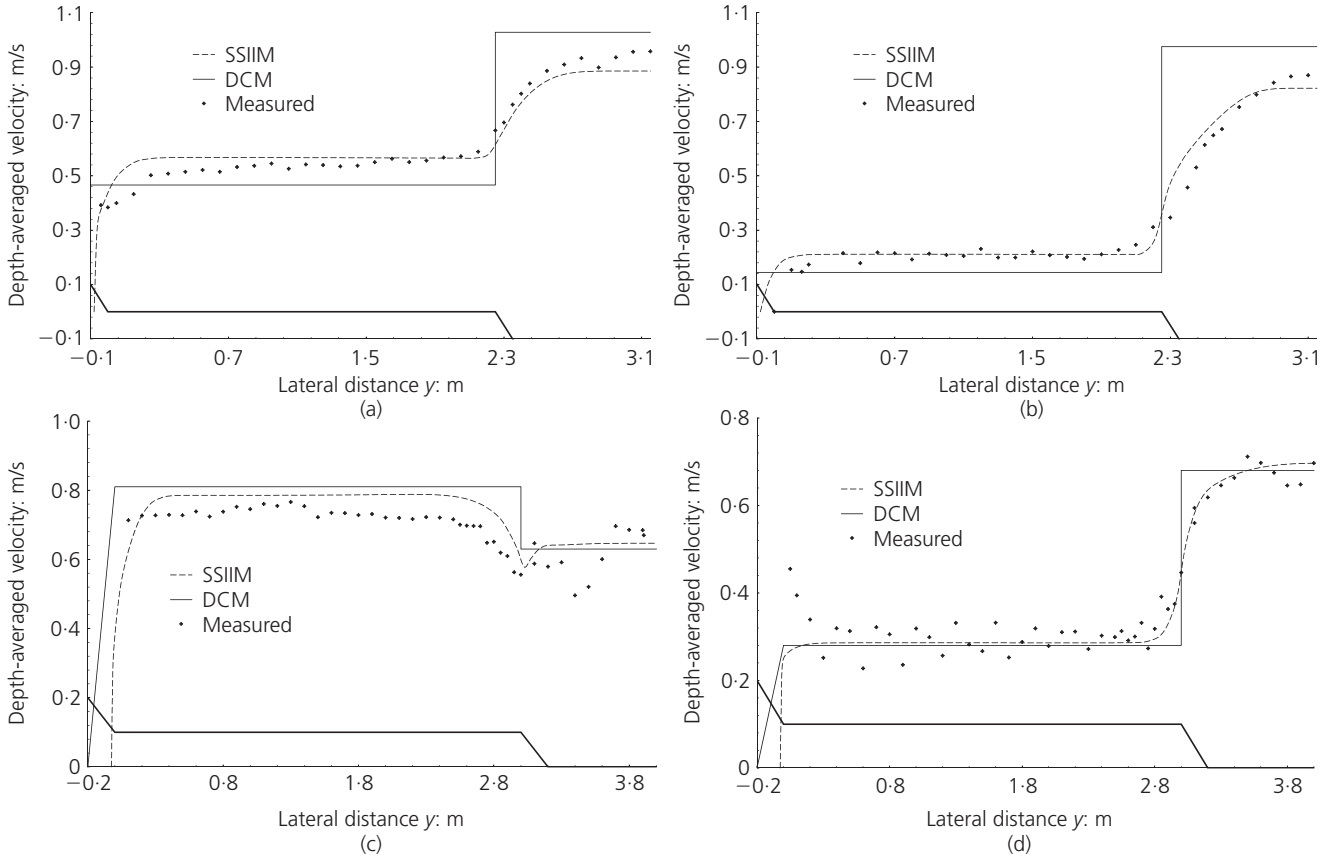


**Figure 7.** Comparison of predicted (SSIIM), calculated (DCM) and measured (FCF) depth-averaged velocities for (a) phase A smooth channel, (b) phase A rough channel, (c) phase C smooth channel and (d) phase C rough channel

While not presented in this paper, the improved approach was also validated against other datasets from the phase A and phase C FCF test series. The results for compound channels with reduced floodplain widths and asymmetric channel sections with isolated floodplain(s) were consistent with those presented.

## 4. Conclusions

An improved approach for estimating uniform flow stage–discharge relationships and velocity distributions in straight compound channels with 3D hydrodynamic codes is presented. The proposed approach is based on inputting (rather than calibrating) physically realistic resistance values and iteratively adjusting downstream water depths until uniform flow conditions within a specified tolerance are established. The approach is therefore predictive. Computed stage–discharge relationships are shown to compare favourably with measured data from the FCF phase A and C straight channels with fixed and mobile beds respectively. Good agreement was observed for both the smooth and roughened floodplain configurations investigated, with predicted stage–discharge relationships being within 5% of measured results.

Divided channel methods (DCMs) neglect the turbulent momentum interaction at the main channel and floodplain interfaces that characterise compound channel flows. The influence of this interaction was assessed by comparing DCM estimates of discharge and velocity with measured values. The momentum exchange for the tested relative depth range is greater for increasing flow depths due to the larger velocity differentials between the main channel and the floodplains. Underestimates of stage for the phase A tests with fixed boundaries and smooth floodplains are approximately 3%, but these increase to approximately 20% for high flows in the roughened floodplain tests. The increased main channel roughness of the phase C mobile bed tests appears to reduce the velocity gradient between the main channel and floodplain zones and the stage for the range of discharges examined is of the order of 3% for both smooth and roughened floodplain tests.

Overestimation of the main channel flow ratio (and corresponding underestimation of the floodplain ratio) by the DCM reflects the above findings. Increasing flow depths result in an increasing overestimation, which is greatest for the roughened floodplain test

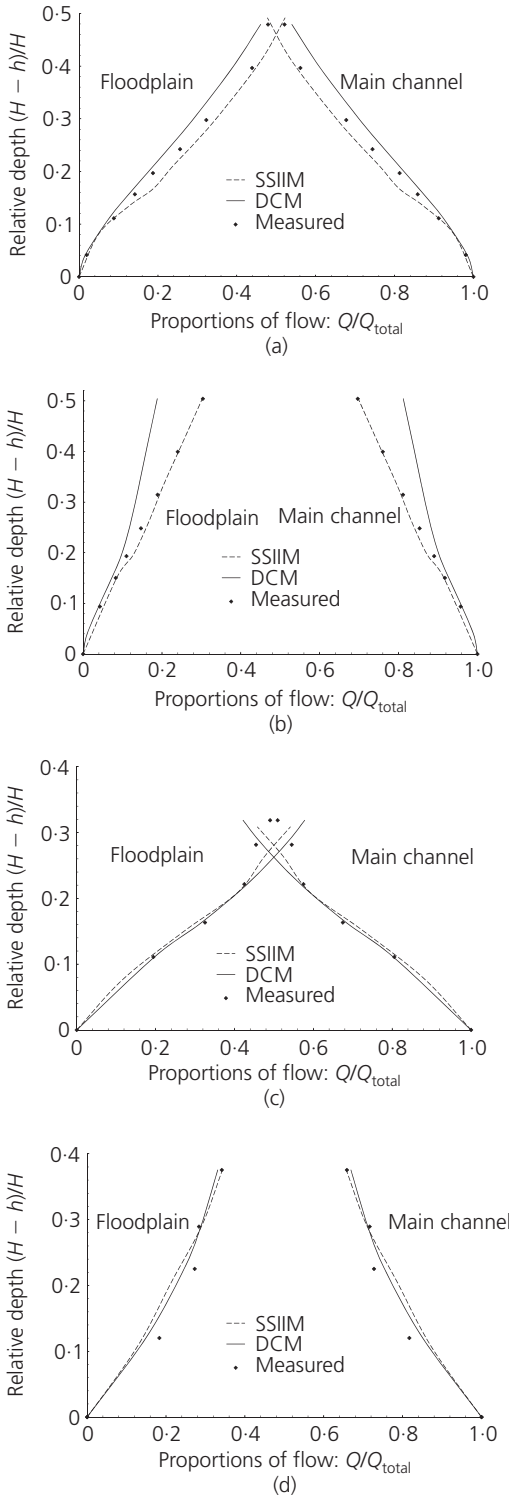


**Figure 8.** Comparison of predicted (SSIIM), calculated (DCM) and measured (FCF) main channel and floodplain flow distribution for (a) phase A smooth channel, (b) phase A rough channel, (c) phase C smooth channel and (d) phase C rough channel

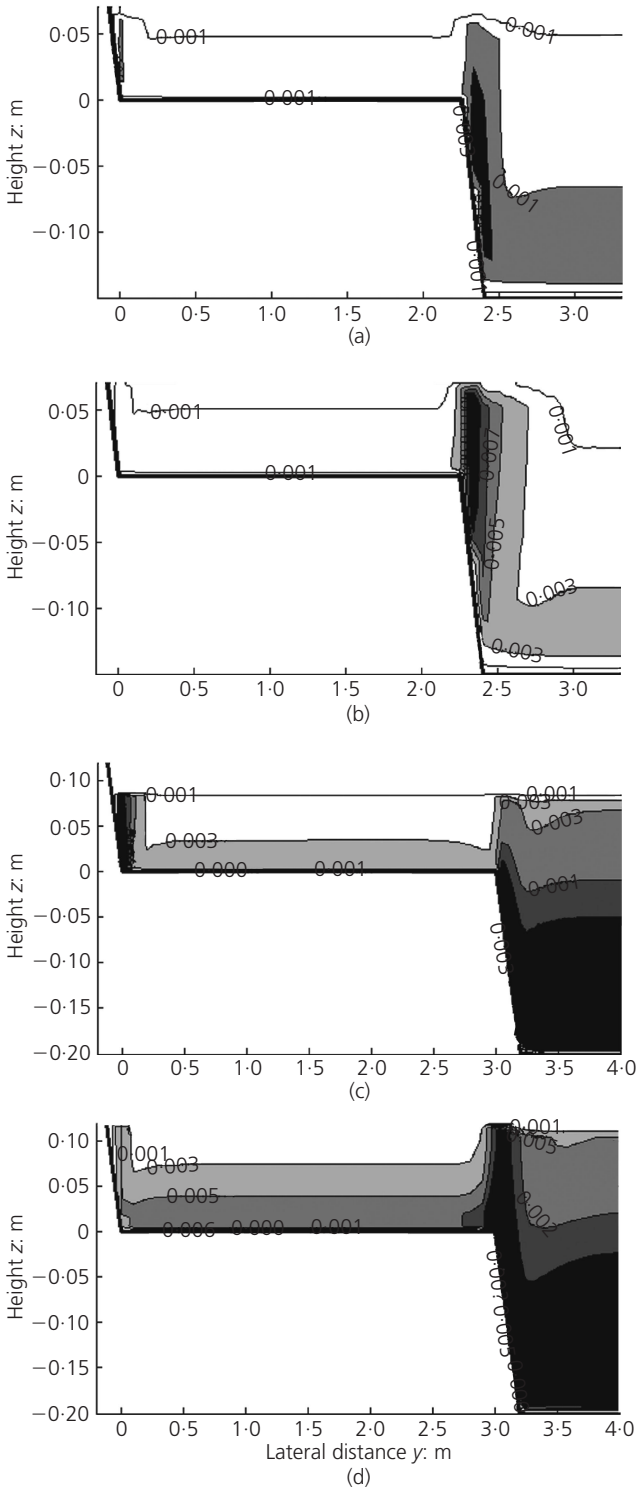


**Figure 9.** Turbulent kinetic energy ($m^2.s^{-2}$) predicted by the new approach applied to SSIIM for (a) phase A smooth channel, (b) phase A rough channel, (c) phase C smooth channel and (d) phase C rough channel

case. Predicted results by the new approach applied to SSIIM provide a better fit to the measured data.

The new approach was successfully validated for straight compound channel flows in fixed and mobile bed channels with both smooth and rod-roughened floodplains. The method in conjunction with SSIIM can successfully predict discharge, velocity and flow distribution measurements in such channels with an acceptable accuracy. Further work is required to determine whether the improved approach can predict these parameters for more complex geometries including both skewed and meandering channel planforms.

## Acknowledgement

The authors wish to acknowledge the financial support made available by the School of Civil, Structural and Environmental Engineering at University College Dublin for facilitating this research.

### REFERENCES

Ackers P (1989) *Resistance Functions for the Wallingford Facility: Rod Roughness*. Water Authority, Wallingford, UK, Technical report no. 2.

Ackers P (1991) *Hydraulic Design of Straight Compound Channels*. HR Wallingford Ltd, Wallingford, UK, Report SR 281.

Cokljat D and Kralj C (1997) On choice of turbulence model for prediction of flows over river bed forms. *Journal of Hydraulic Research* **35(3)**: 355–361.

Colebrook CF (1939) Turbulent flow in pipes, with particular reference to the transition region between the smooth and rough pipe laws. *Journal of the Institution of Civil Engineers* **11(4)**: 133–156.

Cowan WL (1956) Estimating hydraulic roughness coefficients. *Agricultural Engineering* **37(7)**: 473–475.

Demuren AO and Rodi W (1984) Calculation of turbulence-driven secondary motion in non-circular ducts. *Journal of Fluid Mechanics* **140**: 189–222.

Engelund F (1966) Hydraulic resistance of alluvial streams. *Journal of the Hydraulics Division ASCE* **92(2)**: 315–326.

Ettema R (2011) Parametric estimation of an optimal mesh size for depth-averaged numerical flow models. *Proceedings of 34th IAHR World Congress, Brisbane, Australia*, vol. 1, pp. 4227–4234.

Holden AP and James CS (1989) Boundary shear distribution on flood plains. *Journal of Hydraulic Research* **27(1)**: 75–89.

Hollinrake P and Samuels PG (1995) *Flood Discharge Assessment: An Engineering Guide*. HR Wallingford Ltd, Wallingford, UK, Report SR 379.

Jing H, Guo Y, Li C and Zhang J (2009) Three-dimensional numerical simulation of compound meandering open channel flow by the Reynolds stress model. *International Journal for Numerical Methods in Fluids* **59(8)**: 927–943.

Jing H, Li C, Guo Y and Xu W (2011) Numerical simulation of turbulent flows in trapezoidal meandering compound open channels. *International Journal for Numerical Methods in Fluids* **65(9)**: 1071–1083.

Kang H and Choi SU (2006) Reynolds stress modelling of rectangular open-channel flow. *International Journal for Numerical Methods in Fluids* **51(11)**: 1319–1334.

Keller RJ and Rodi W (1988) Prediction of flow characteristics in main channel/flood plain flows. *Journal of Hydraulic Research* **26(4)**: 425–441.

Keller RJ and Wong WT (1986) Analytical and experimental study of flow characteristics in open channels of compound cross-section. *Proceedings of 9th Australasian Fluid Mechanics Conference, Auckland, New Zealand*, pp. 354–357.

Knight DW and Demetriou JD (1983) Flood plain and main channel flow interaction. *Journal of Hydraulic Engineering* **109(8)**: 1073–1092.

Knight DW and Hamed ME (1984) Boundary shear in symmetrical compound channels. *Journal of Hydraulic Engineering* **110(10)**: 1412–1430.

Knight DW and Shiono K (1990) Turbulence measurements in a shear layer region of a compound channel. *Journal of Hydraulic Research* **28(2)**: 175–196.

Knight DW, Demetriou JD and Hamed ME (1984) Boundary shear in smooth rectangular channels. *Journal of Hydraulic Engineering* **110(4)**: 405–422.

Knight DW, Brown F, Valentine E *et al.* (1999) The response of straight mobile bed channels to inbank and overbank flows. *Proceedings of the Institution of Civil Engineers – Water, Maritime and Energy* **136(4)**: 211–224.

Lambert MF and Myers WR (1998) Estimating the discharge capacity in straight compound channels. *Proceedings of the Institution of Civil Engineers – Water, Maritime and Energy* **130(2)**: 84–94.

Larsson R (1988) Numerical simulation of flow in compound channels. *Proceedings of 3rd International Symposium on Refined Flow Modelling and Turbulence Measurements, Tokyo, Japan*, pp. 537–544.

Launder BE and Spalding DB (1974) The numerical computation of turbulent flows. *Computer Methods in Applied Mechanics and Engineering* **3(2)**: 269–289.

Limerinos JT (1970) *Studies of Flow in Alluvial Channels. Determination of the Manning Coefficient from Measured Bed Roughness in Natural Channels*. California Department of Water Resources. Sacremento, CA, USA, Geological Survey Water Supply Paper 1898-B.

Martin LA and Myers WRC (1991) Measurement of overbank flow in a compound river channel. *Proceedings of the Institution of Civil Engineers – Water, Maritime and Energy* **91(2)**: 645–657.

Matthes GH (1947) Macroturbulence in natural stream flow. *Transactions of AGU* **28(2)**: 255–265.

Morvan H, Knight D, Wright N, Tang X and Crossley A (2008) The concept of roughness in fluvial hydraulics and its formulation in 1D, 2D and 3D numerical simulation models. *Journal of Hydraulic Research* **46(2)**: 191–208.

Myers WRC (1978) Momentum transfer in a compound channel. *Journal of Hydraulic Research* **16(2)**: 139–150.

Olsen NRB (2004) *SSIIM User Manual*. Norwegian University of Science and Technology, Trondheim, Norway.

Patankar SV (1980) *Numerical Heat Transfer and Fluid Flow.* McGraw-Hill, New York, NY, USA.

Rameshwaran P and Naden PS (2004) Modelling turbulent flow in two-stage meandering channels. *Proceedings of the Institution of Civil Engineers – Water Management* **157(3)**: 159–173.

Rodi W (1980) *Turbulence Models and their Application in Hydraulics, A State of the Art Review.* IAHR, Delft, The Netherlands, 1980.

Samuels PG (1989) The hydraulics of two stage channels – review of current knowledge. *Proceedings of Conference of River Engineers, Loughborough, UK*.

Samuels PG (1990) Cross-section location in 1-D models. *International Conference on River Flood Hydraulics, Wallingford, UK*. Wiley, New York, USA, pp. 339–350.

Schlichting H (1979) *Boundary Layer Theory.* McGraw-Hill, New York, NY, USA.

Sellin HJ (1964) A laboratory investigation into the interaction between the flow in the channel of a river and that over its floodplain. *La Houille Blanche* **7**: 703–801.

Shen HW, Fehlman HM and Mendoza C (1990) Bed form resistances in open channel flows. *Journal of Hydraulic Engineering* **116(6)**: 799–815.

Shiono K and Knight DW (1991) Turbulent open-channel flows with variable depth across the channel. *Journal of Fluid Mechanics* **222(6)**: 617–646.

Simons DB and Richardson AM (1961) Forms of bed roughness in alluvial channels. *Journal of the Hydraulics Division ASCE* **87(3)**: 87–105.

Sofialidis D and Prinos P (1998) Compound open-channel flow modeling with nonlinear low-Reynolds $k$–$\varepsilon$ models. *Journal of Hydraulic Engineering* **124(3)**: 253–262.

Van Rijn LC (1984) Sediment transport. Part III: Bed forms and alluvial roughness. *Journal of the Hydraulics Division ASCE* **110(12)**: 1733–1754.

Wilcox DC (1993) *Turbulence Modelling for CFD.* DCW Industries, Inc., La Canada, CA, USA.

Wilson CAME, Boxall JB, Guymer I and Olsen NRB (2003a) Validation of a three-dimensional numerical code in the simulation of pseudo-natural meandering flows. *Journal of Hydraulic Engineering* **129(10)**: 758–768.

Wilson CAME, Stoesser T, Olsen NRB and Bates PD (2003b) Application and validation of numerical codes in the prediction of compound channel flows. *Proceedings of the Institution of Civil Engineers – Water and Maritime Engineering* **156(2)**: 117–128.

Wormleaton PR and Ewunetu M (2006) Three-dimensional $k$–$\varepsilon$ numerical modelling of overbank flow in a mobile bed meandering channel with floodplains of different depth, roughness and planform. *Journal of Hydraulic Research* **44(1)**: 18–32.

Wormleaton PR, Allen J and Hadjipanos P (1982) Discharge assessment in compound channel flow. *Journal of the Hydraulics Division ASCE* **108(9)**: 975–994.

Xiaohui S and Li CW (2002) Large eddy simulation of free surface turbulent flow in partly vegetated open channels. *International Journal for Numerical Methods in Fluids* **39(10)**: 919–938.